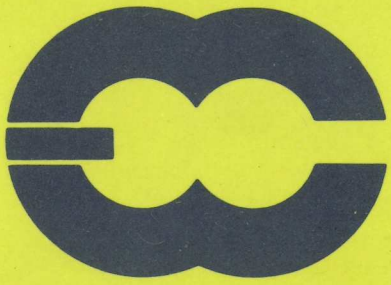

European Centre
for Medium Range
Weather Forecasts

Test of a Lateral Boundary Relaxation Scheme in a Barotropic Model.

Internal Report 3.
Research Dept.

February 77.

Centre Européen pour les Prévisions Météorologiques
a Moyen Terme

Europäisches Zentrum Für Mittelfristige Wettervorhersagen

TEST OF A LATERAL BOUNDARY RELAXATION SCHEME IN A BAROTROPIC MODEL.

By

P. Källberg

European Centre for Medium Range Weather Forecasts, Bracknell.

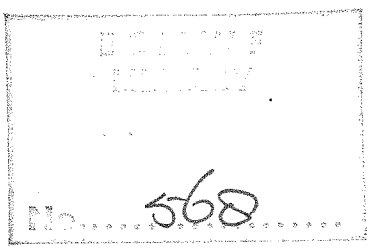

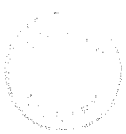

Internal report 3,
Research Department.

1. Introduction

A limited area version of the first ECMWF gridpoint model is currently being developed. The main purpose is to provide a tool for high resolution tests of different physical parameterizations with reasonable demands on computing power. A pragmatic, engineering approach has been taken, and in the present report some barotropic tests of the adopted boundary scheme are described.

The full mathematical problem of time-dependent lateral boundary conditions for a limited area primitive equations baroclinic model is complicated. To be sure that there are stable solutions, a minimum requirement is that the corresponding linear problem is well posed. This means that the number and form of the boundary conditions must be such that the solution is uniquely defined at the boundary. If the time derivative of a variable may be computed entirely from the interior, it should not be prescribed from the surroundings. (See for instance Sundström, 1973). For a barotropic atmosphere, with the dependent variables u, v and ϕ, this means that two conditions have to be satisfied at the inflow boundary, but only one at the outflow. The conditions can be such that the tangential velocity is prescribed at inflow points only, and some combination of the normal velocity and the geopotential at all points. In a baroclinic, hydrostatic model atmosphere, the boundary conditions must also give relations between variables at different pressure (or σ-) levels. It can in fact be shown that a correct set of boundary conditions should be specified separately for each vertical eigen-mode of the model. This is, to say the least, an impractical procedure, and two different approaches to circumvent the problem can be distinguished. One method is to separate inflow and outflow boundary points at each level and apply some approximate simplified extrapolation from inside at the latter. This is done successfully by several groups, for instance GFDL (Miyakoda and Rosati, 1977). A still simpler approach is to specify all variables at all boundary points, thus deliberately overspecifying the boundary conditions. The resulting instabilities then have to be damped by heavy diffusion. As an alternative to diffusion, Davies (1976) suggested a Newtonian relaxation technique in which the interior, limited area, variables are smoothly adjusted towards their prescribed boundary values. A somewhat simplified version of his method has been used in the present work.

2. Barotropic test model

The model used is a barotropic version of the first ECMWF gridpoint model. (Burridge, 1977). With additional terms for the boundary treatment, the model is defined in conventional notations by

$$\frac{\partial u}{\partial t} - \eta \cdot v + \frac{\partial H}{\partial x} = K \cdot (u - \tilde{u}) \tag{1}$$

$$\frac{\partial v}{\partial t} + \eta \cdot u + \frac{\partial H}{\partial y} = K \cdot (v - \tilde{v}) \tag{2}$$

$$\frac{\partial \phi}{\partial t} + \frac{\partial}{\partial x}(\phi u) + \frac{\partial}{\partial y}(\phi v) = K \cdot (\phi - \tilde{\phi}) \tag{3}$$

$$\eta = f + \frac{\partial v}{\partial x} - \frac{\partial u}{\partial y} \tag{4}$$

$$H = \phi + \frac{1}{2}(u^2 + v^2) \tag{5}$$

In the right hand side, $\tilde{u}$, $\tilde{v}$ and $\tilde{\phi}$ are the externally prescribed forcings. K(x,y) is a relaxation coefficient which is non-zero only in a boundary zone surrounding the limited area. In Davies' original formulation, equations (1) and (2) included additional terms of the type

$$F_u = \int_{Y_i}^{Y_b} \frac{\partial K}{\partial y} (u - \tilde{u})\, dy \tag{6}$$

where the integration is from some interior point, Y_i where $K = \partial K/\partial y = 0$ to the boundary, Y_b. The effect of the integral terms is to adjust the vorticity of the limited area towards its prescribed boundary values. The integrals, however, complicate the coding of the global baroclinic model to such an extent that they have been disregarded here. Using explicit, leap-frog time integration, the finite difference equation corresponding to (1) is

$$u^{\tau+1} = (1-\alpha)(u^{\tau-1} + 2\Delta t \cdot \mathcal{D}u^{\tau}) + \alpha \cdot \tilde{u}^{\tau+1} \qquad (7)$$

with identical equations for $v^{\tau+1}$ and $\phi^{\tau+1}$.
The superscripts denotes the time level, and

$$\alpha = \frac{K \cdot 2\Delta t}{1 + K \cdot 2\Delta t} \qquad (8)$$

Since K is large in some parts of the boundary zone, implicit application of $K \cdot (u - \tilde{u})$ at the time level $\tau+1$ is required for stability.

$\mathcal{D}u^{\tau}$ is the interior tendency. In the staggered, Arakawa type C, mesh used here as well as in the baroclinic model $\mathcal{D}u^{\tau}$ is defined by: (in conventional finite difference symbolism)

$$\mathcal{D}u^{\tau} = -\left\{-\overline{\eta}^{y} \cdot \overline{v}^{xy} + D_{ox}\left[\phi + \frac{1}{2}\left(\overline{u^2}^{x} + \overline{v^2}^{y}\right)\right]\right\} \qquad (9)$$

The boundary forcings, $\tilde{u}$, $\tilde{v}$ and $\tilde{\phi}$ are interpolated spatially and temporally for each point in the boundary zone from a coarse mesh forecast. The spatial interpolation is made using a high order procedure by Shapiro (1973). The basic idea of the scheme is to restore as much as possible of the unwanted damping resulting from linear interpolation. This is achieved by the successive application of a restoration operator

$$z_i^{*} = z_i + \frac{S}{2}\left(z_{i-1} - 2 \cdot z_i + z_{i+1}\right) \qquad (10)$$

where S is determined so as to maximize the restoration of the damped amplitudes without amplifying any component beyond its original value. Two successive restorations, which amounts to an eight-point interpolation, are made in the x- and y- directions separately. The temporal interpolation is linear.

3. Results and discussion

In the first experiment a pure gravity wave (no rotation of the earth) was integrated in a 40 x 40 points mesh with the mesh size of 10 km. The lateral boundary conditions were constant in time and given by

$$\tilde{u} = \tilde{v} = 0$$
$$\tilde{\phi} = \phi_0 = \text{const.} \qquad (11)$$

The initial condition was a height disturbance in the shape of a hump at the centre of the area, and no initial winds. Ideally this disturbance should move outwards through the boundaries and disappear without reflection. An integration up to +50 minutes, timestep 10 sec, without boundary relaxation is shown in figure 1. It can be seen that the boundaries reflect all the wave energy, and waves remain in the area throughout the integration. In figure 2 a 6-point wide relaxation zone with a linear spatial variation of the relaxation coefficient, α, has been added. Now the boundary zones absorb the waves with very little reflection. The good absorbtion of gravity waves is further emphasized in figure 3. It shows the variation with the time of the (very small) kinetic energy of the wave disturbance. After 30 minutes no trace of the wave can be detected.

In a second series of experiments, geostrophically balanced planetary waves in a cyclic β-plane channel with Δs = 300 km were integrated to provide external boundary forcing for an embedded limited area covering 40 x 40 points, with Δs = 100 km. A coarse mesh integration to +60 days was stable without any smoothing in time or space, and no smoothing apart from the relaxation itself has been applied in the limited area integrations. In figure 4 the initial fields are shown for the full cyclic area with the limited area outlined by the inner frame. For comparison with later figures a +48 hour forecast in the full cyclic channel with Δs = 100 km and Δt = 100 sec is shown in figure 5. A +48 hour integration in the limited area without boundary relaxation is shown in figure 6. The overspecification of the boundary data produces disastrous noise, particularly in the tangential velocity at the outflow boundaries. This is demonstrated by the vorticity

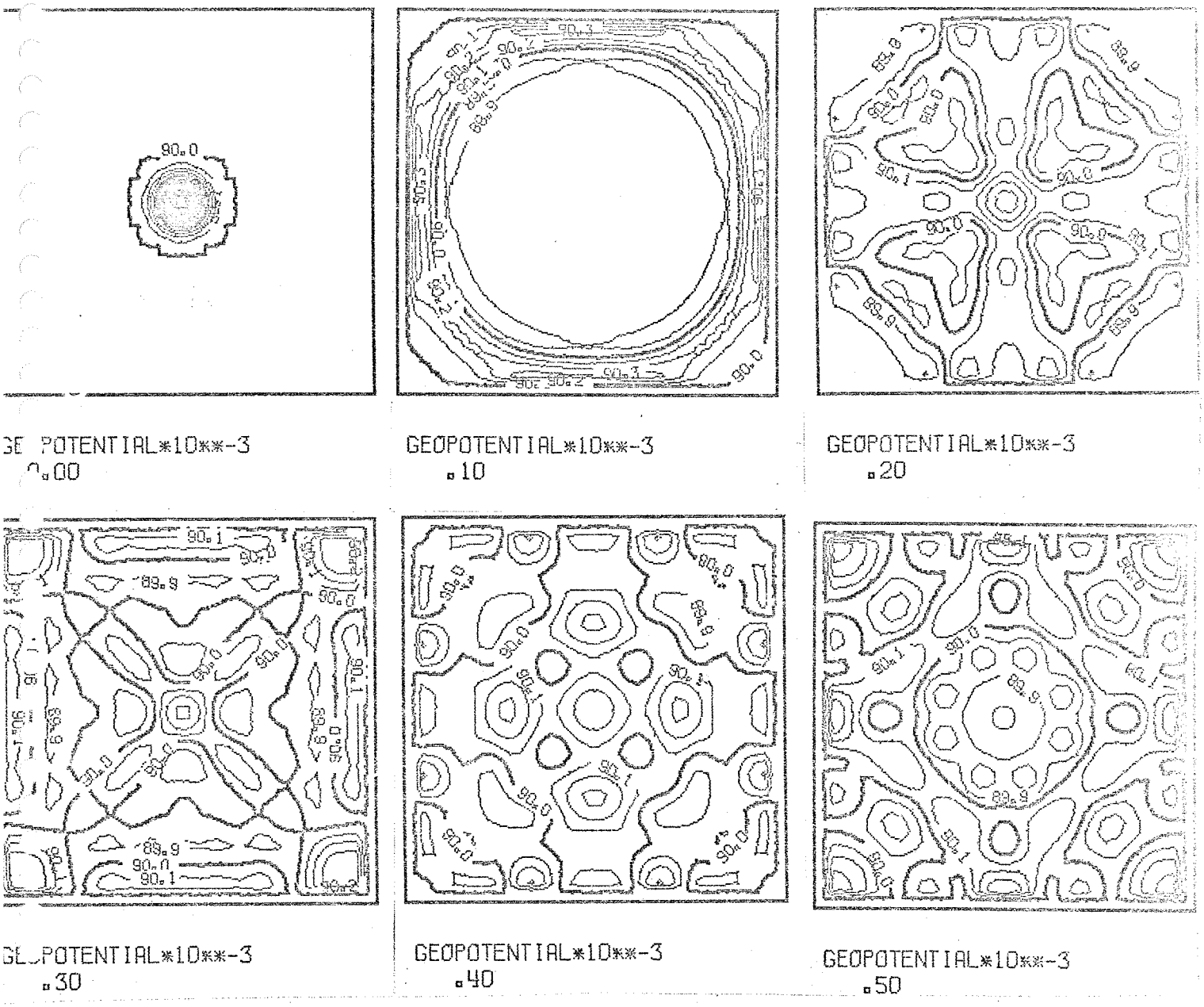

Figure 1.

Geopotential ($m^2 sec^2$) at 10 minute intervals.
Without boundary relaxation.
40 x 40 points, meshsize 10 km, timestep 10 sec.

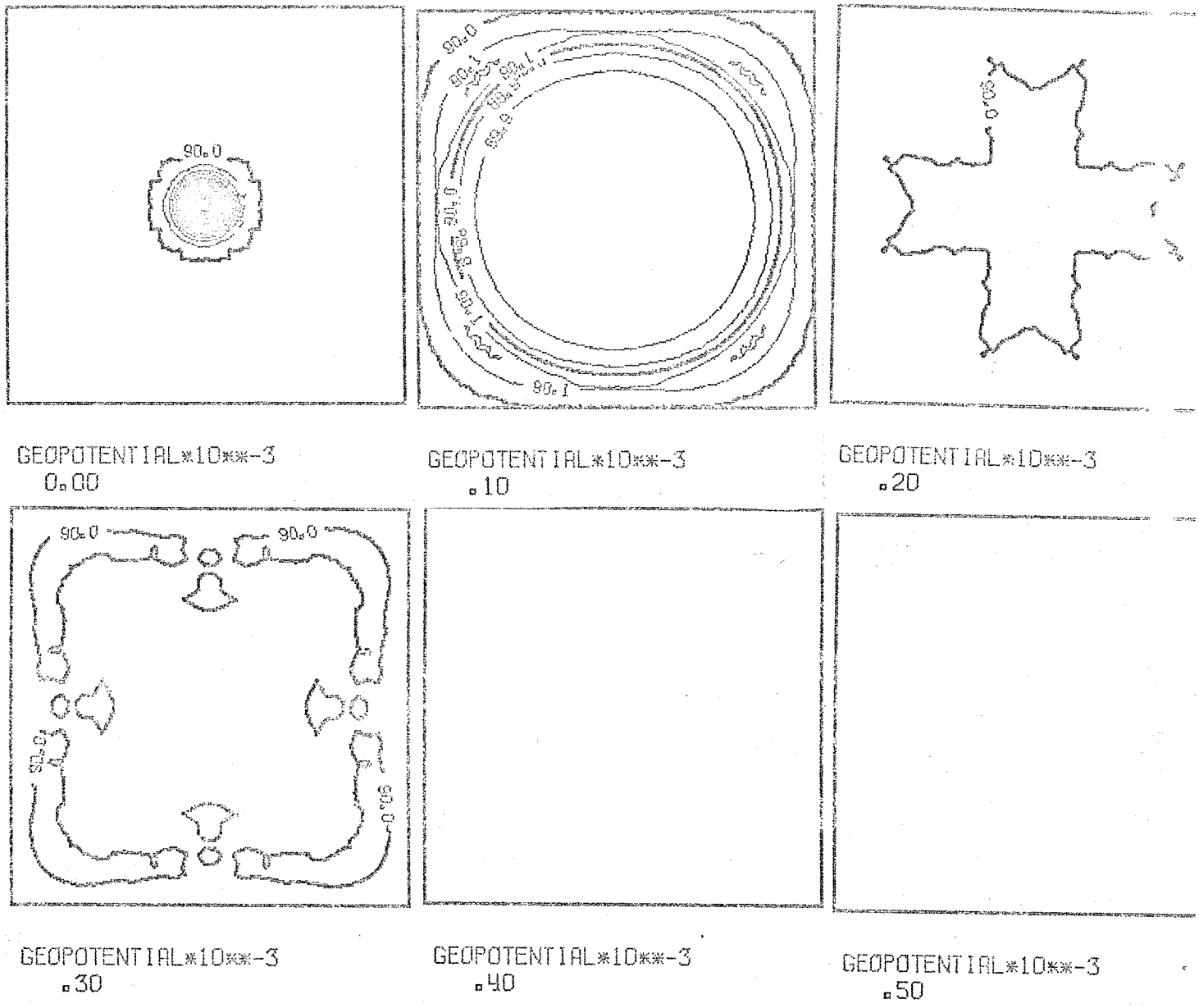

Figure 2.

As figure 1 but with boundary relaxation. The isoline marked 90.0 denotes 1% of the initial amplitude.

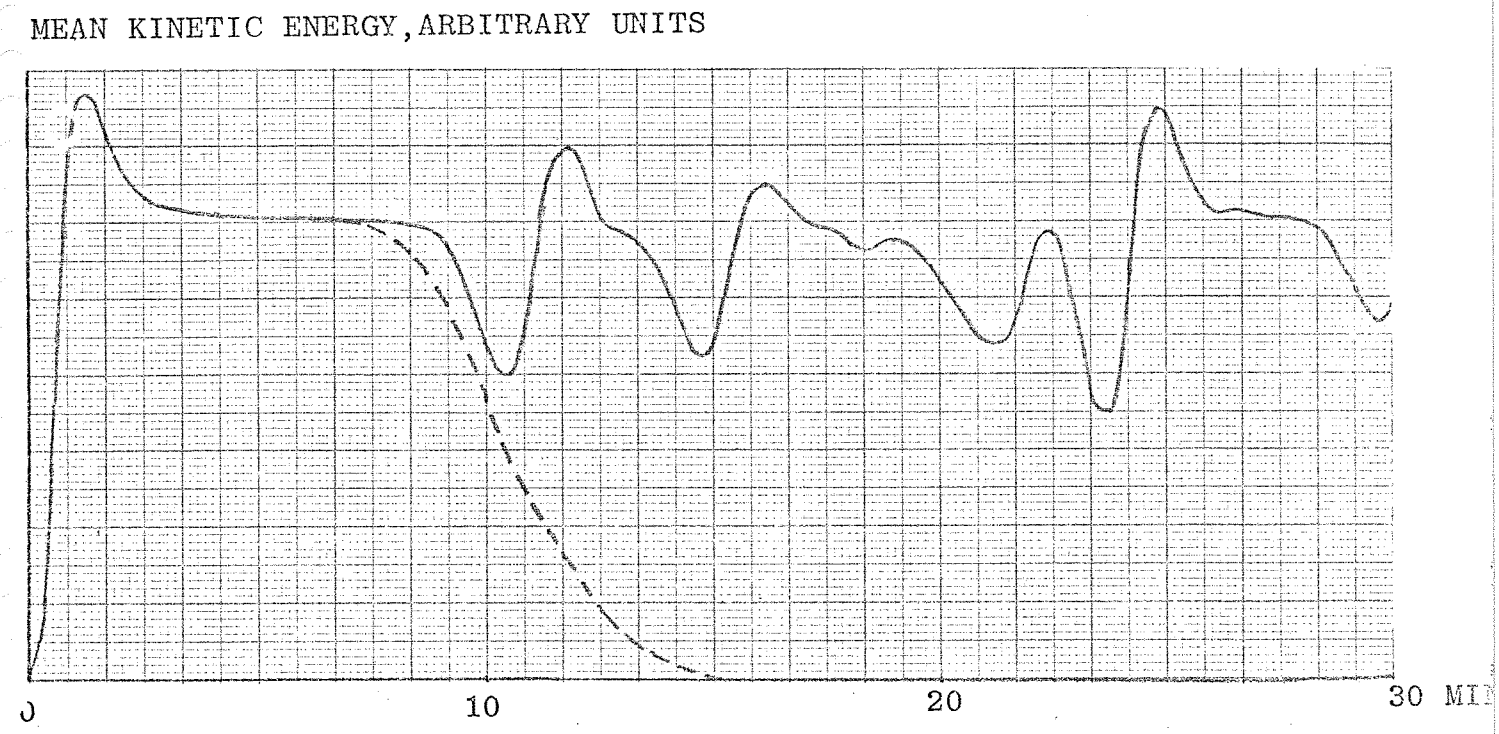

Figure 3.

Disturbance kinetic energy as function of time, without relaxation (full line) and with relaxation (dashed line).

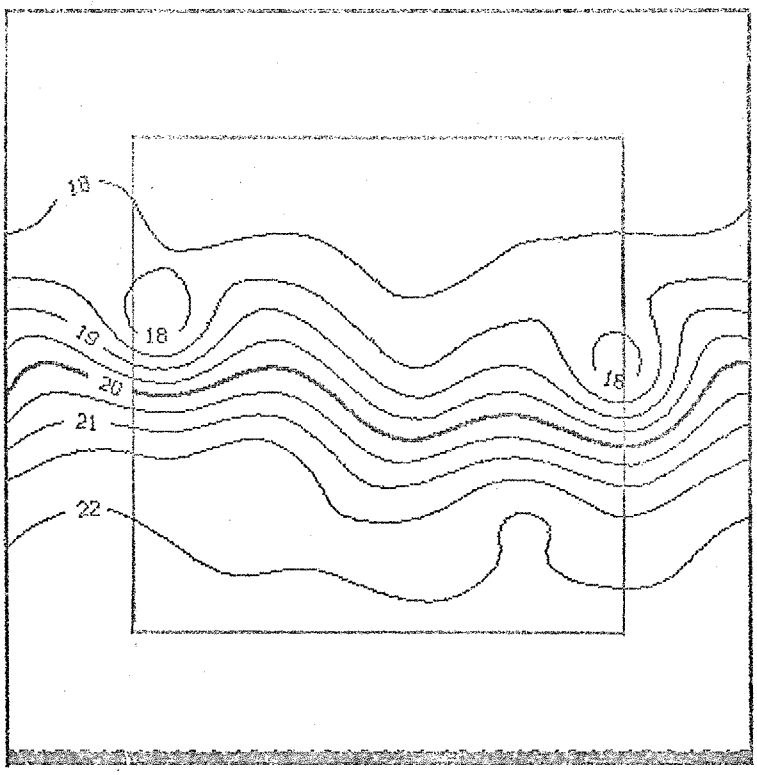

Figure 4.

Initial fields in the full cyclic area. The limited area is outlined by the inner frame. Winds in $msec^{-1}$. Geopotential in m^2sec^2.

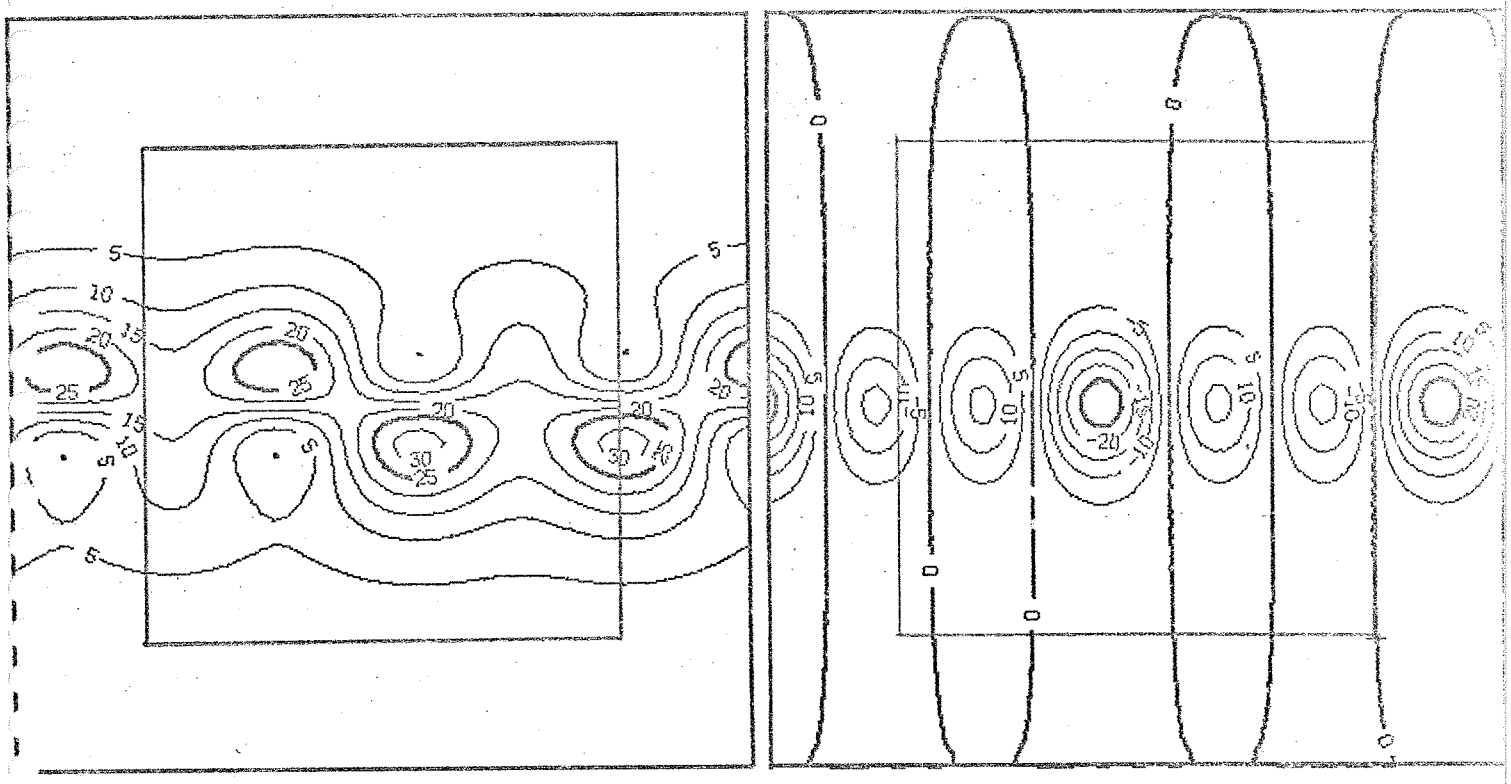

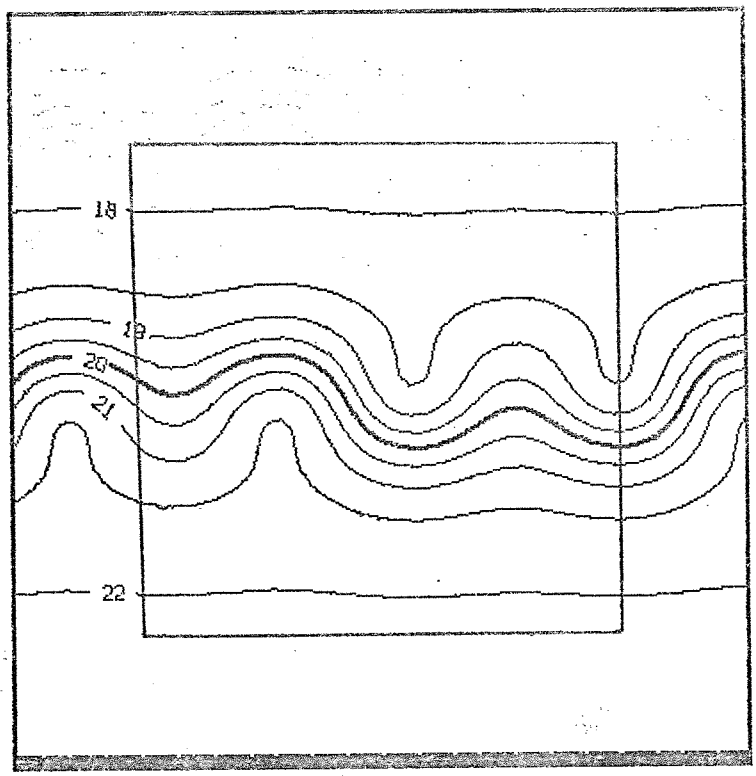

Figure 5.

+48 hour forecast in the full cyclic area. Fine mesh 100 km, timestep 100 sec. The limited area is outlined by the inner frame. Winds in $msec^{-1}$. Geopotential in m^2sec^2.

fields at +24 hour and +48 hour, figure 7. The noise is spreading upstream and at +48 hour it covers a major part of the area. Detailed plots of the +24 hour tangential velocity at each point of the outflow part of a certain "latitude" are shown in figures 8. In figure 8a the aforementioned instability in the tangential velocity is seen close to the boundary. In figure 8b an 8 points wide boundary zone has been added where α decreases linearly from $\alpha = 1$ at the boundary to $\alpha = 0$ in the interior.

The only effect of the relaxation is a displacement of the noise generation to the inner part of the zone. This indicates that the relaxation coefficient is too large in the major part of the zone. Indeed $\alpha = 0.5$ corresponds to an e-damping time of 10 minutes when the timestep is 100 seconds. This damping was suitable for the high frequency gravity waves in figure 2, but is clearly too large for Rossby waves with frequencies of the order 1 day^{-1}.

An α - profile specified by

$$\alpha_{tanh} = 1 - \tanh(a \cdot j) \qquad (12)$$

where j is the number of grid-distances to the closest boundary, and a is a constant gives more realistic damping in the zone, see table 1.

j	lin	e-damping, days	tanh	e-damping, days
0	1.000	0.11	1.000	0.11
1	0.875	0.12	0.538	0.16
2	0.750	0.13	0.238	0.29
3	0.625	0.14	0.095	0.64
4	0.500	0.17	0.036	1.60
5	0.375	0.20	0.013	4.20
6	0.250	0.28	0.005	11.3
7	0.125	0.50	0.002	30.6
8	0.000	∞	0.000	∞

Table 1. e-damping time in days for the two different α - profiles α lin and α tanh. $a = 0.5$.

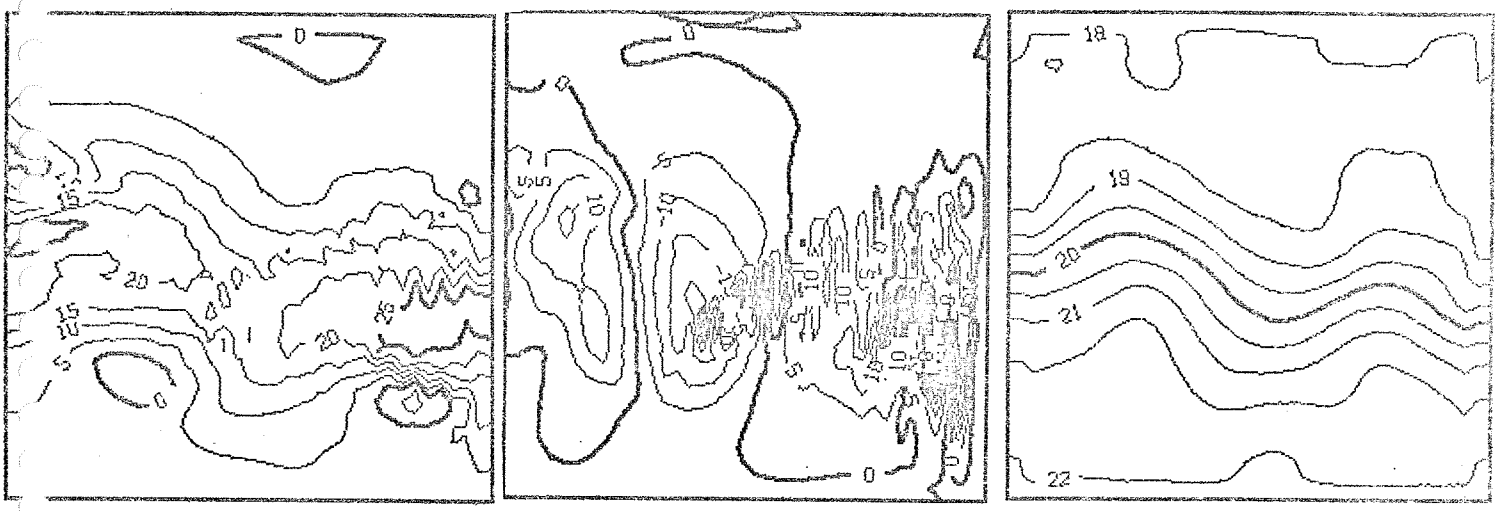

Figure 6.

+48 hour forecast, limited area. Without boundary relaxation. Other data as fig.5.

Figure 7.

+24 hour and +48 hour vorticity in sec^{-1}. Without relaxation.

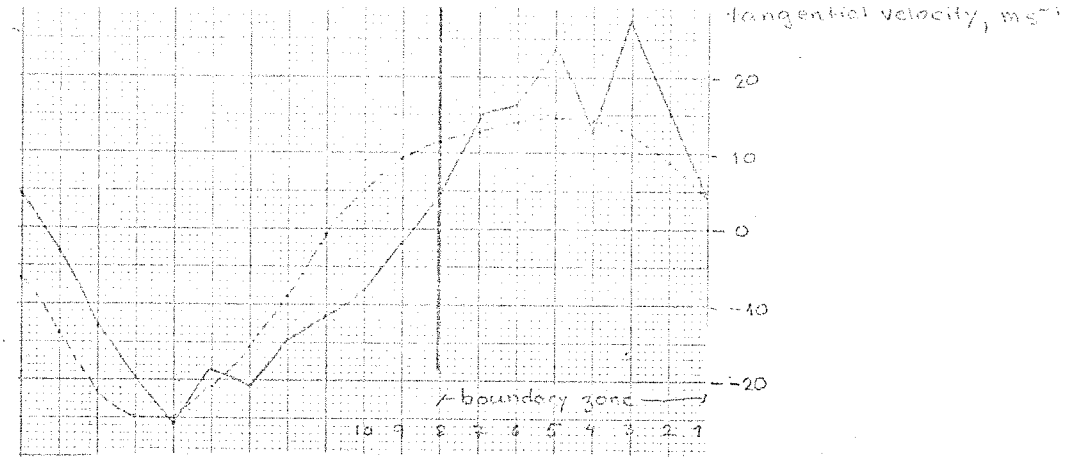

Figure 8a.

Tangential velocity ($msec^{-1}$) at the outflow boundary of one row of gridpoints. Dashed line interpolated forcing. Full line limited area forecast without relaxation.

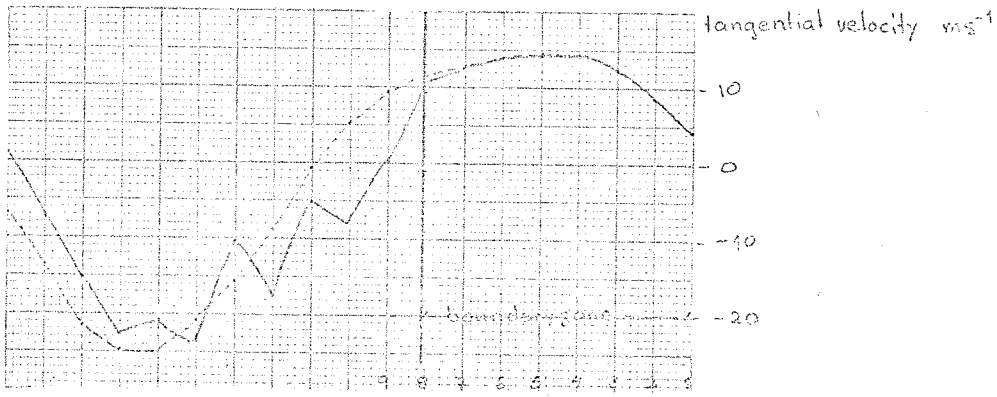

Figure 8b.

As fig. 8a but with relaxation. Relaxation coefficient linear.

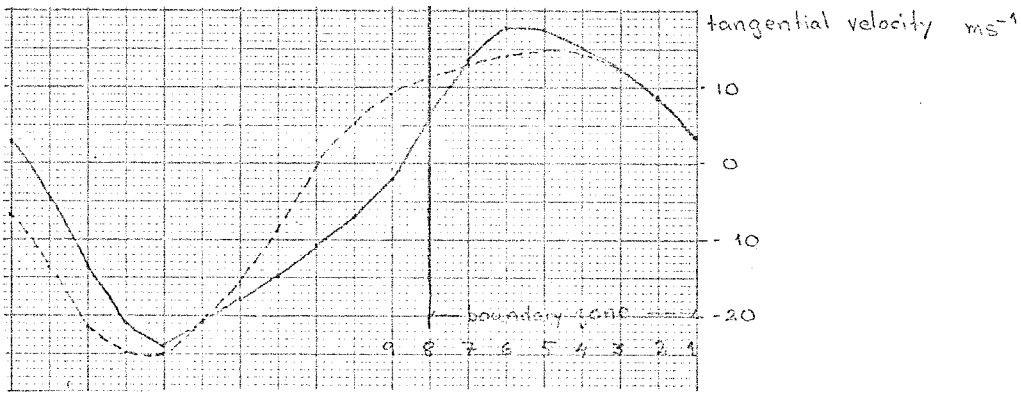

Figure 8c.

As fig. 8b but tanh-shaped relaxation coefficient.

Use of the tanh-profile for α in the boundary zone results in the tangential velocities in figure 8c. The interior now adjusts smoothly to the external forcing. +24 hour and +48 hour forecasts with the tanh-profile in a somewhat narrower, 6-point boundary zone are shown in figures 9 and 10, upper parts. Comparison with the coarse mesh integration in the lower part of the figures shows that the boundary scheme successfully transfers the external forcing to the limited area. The severe boundary noise in the vorticity field in figure 7 disappears with the relaxation procedure. Figure 11 shows the +24 hour vorticity from the fine mesh full area integration (left) and the corresponding limited area integration (right). A small scale computational mode has developed, but since it is very similar in both figures, it is not generated by the boundary or the interpolation. Indeed a slight spatial filter eliminates this noise, but in order not to reduce possible boundary induced noise, no filtering was done in these experiments.

Since the shorter wave component in the initial data is only 1800 km, the coarse mesh forecast of this wave has too low phase velocity and too small amplitude when compared with the fine mesh, cyclic run in figure 5. 1800 km corresponds to only 6 points in the coarse mesh and 18 in the fine mesh. The different phase velocities causes deformation of the limited area wave both at the inflow side, where it is stretched, and at the outflow side, where it is shortened. This effect is unavoidable in any limited area formulation using overspecified boundary conditions, and it limits the practical time limit of integration of such a model (Kreiss and Oliger, 1973).

Some further integrations were made to determine the necessary width of the relaxation zone. With tanh-profiles of α, 8- and 6-point zones performed well, but a narrower 4-point zone was not able to eliminate the boundary induced vorticity noise. Updating of the boundary forcing was usually made every hour, but updating every sixth hour was not markedly inferior to hourly updating.

The limited area divergence forecasts were contaminated with shortwave noise in the boundary zone. This disturbance did not, however, propagate into the interior, see figure 12. The cause of the divergence noise was found to be the spatial interpolation of the boundary forcing data, u, v. Even if the Shapiro scheme is designed to minimize the generation of spurious short wavelengths in the interpolated fields it does not

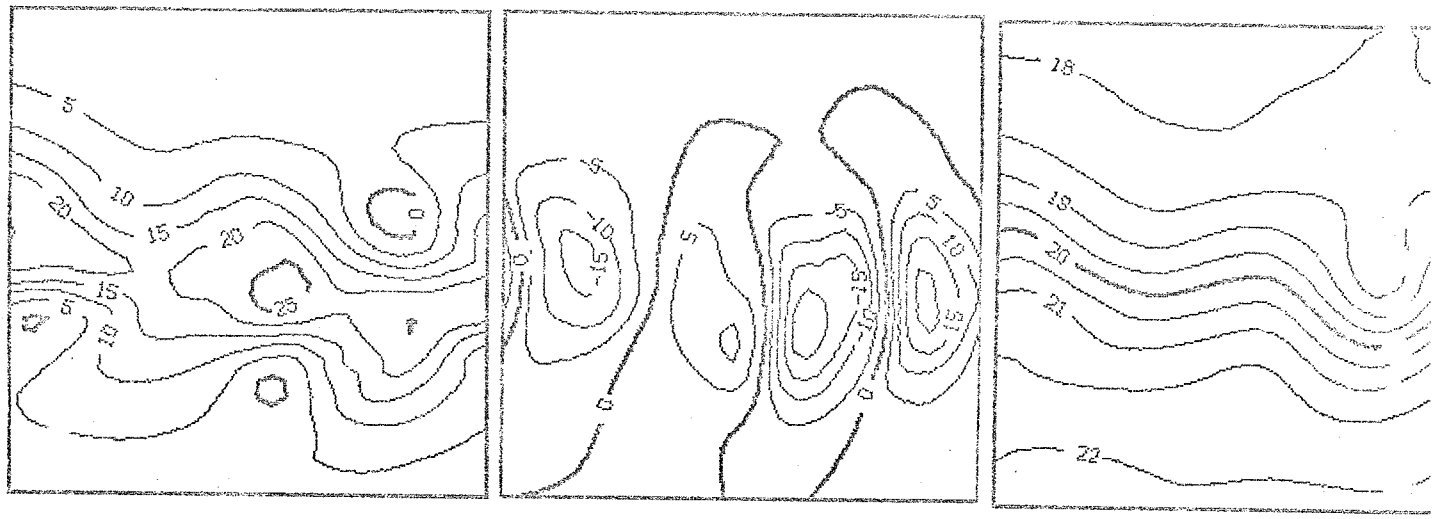

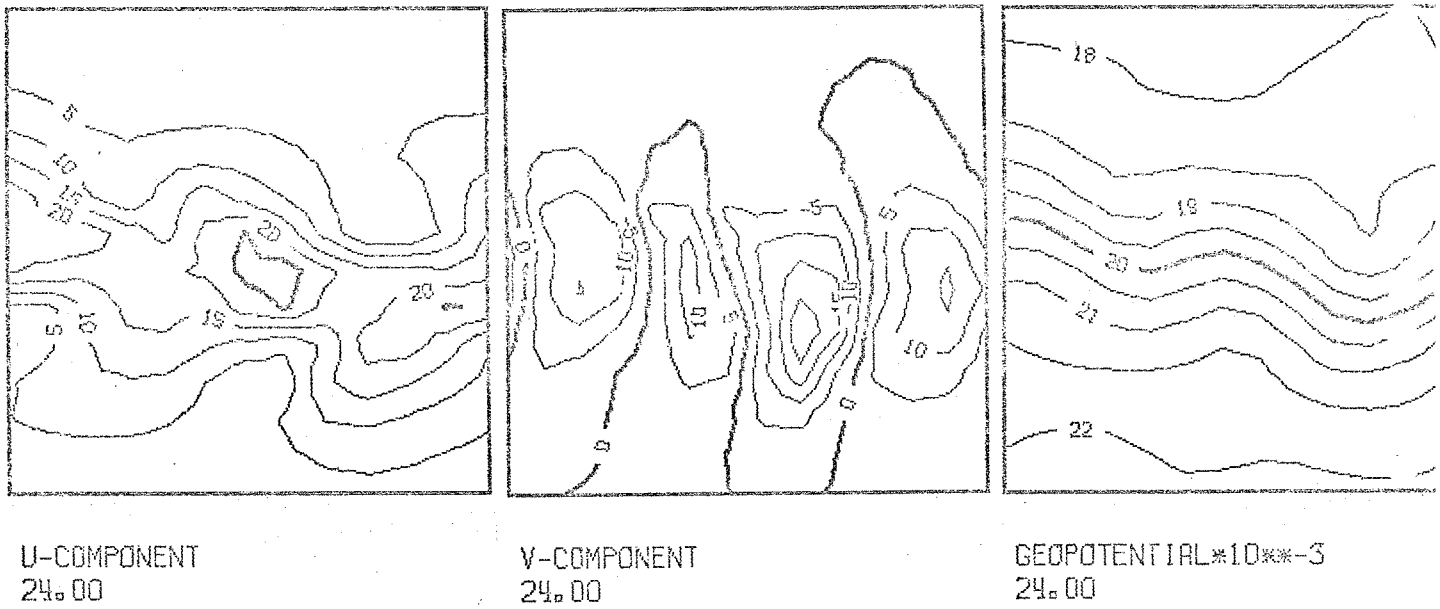

Figure 9.

+24 hour limited area forecast (upper part) with tanh-relaxation.
+24 hour coarse mesh forecast over the limited area (lower part).
Isolines as in fig.5.

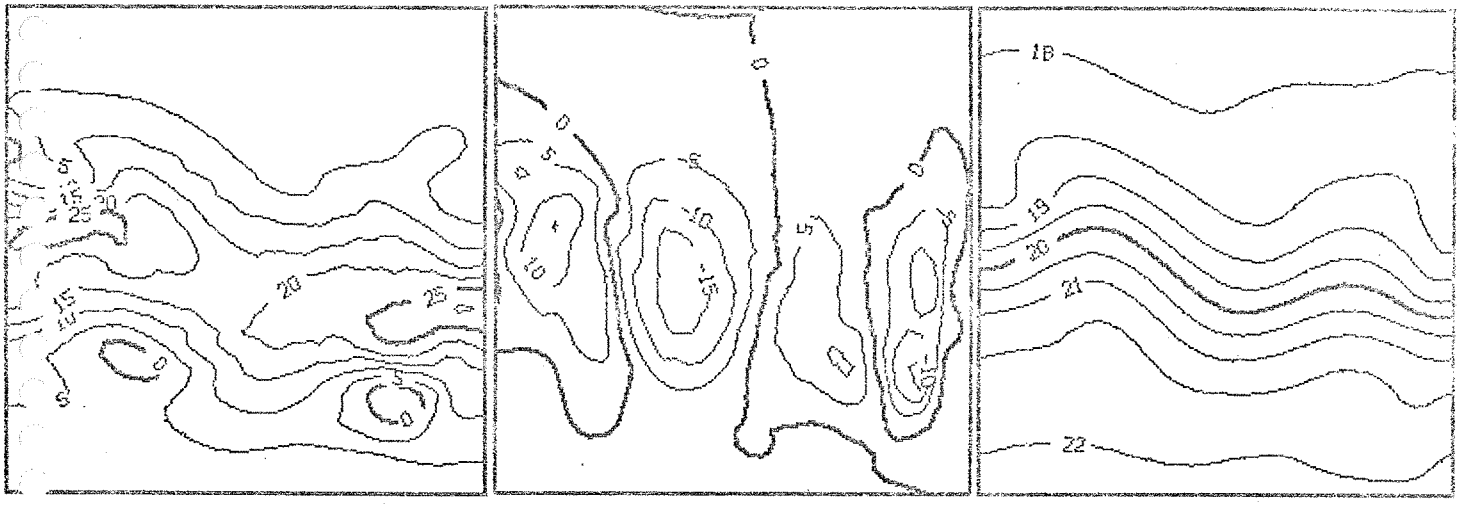

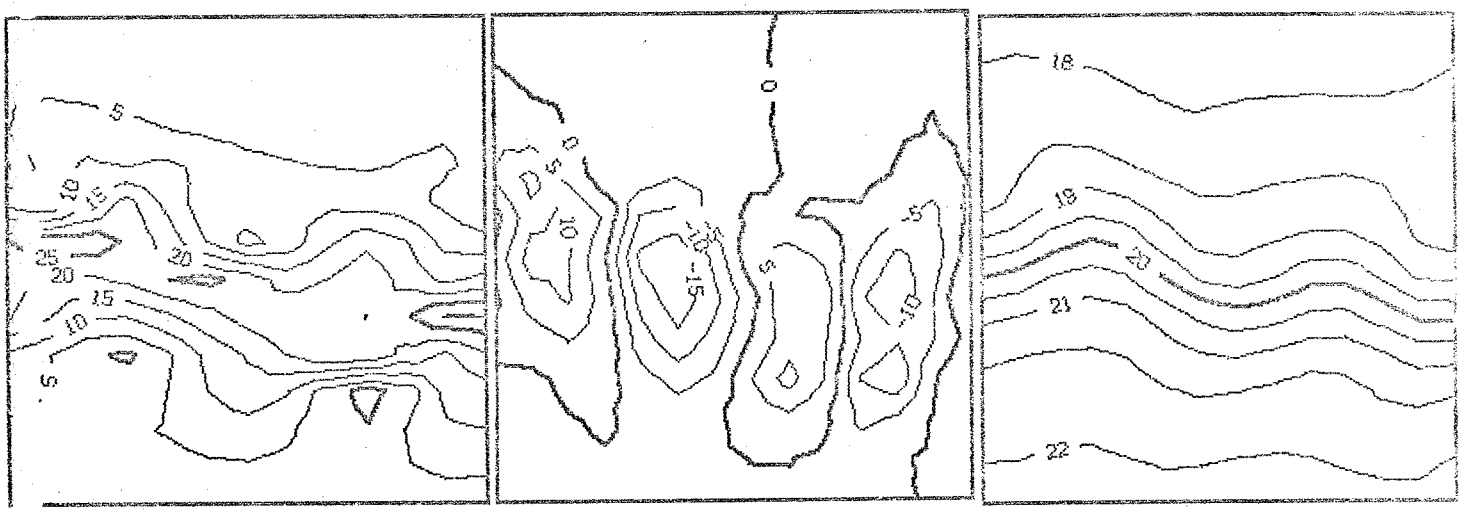

Figure 10.

As fig. 9 but for +48 hour.

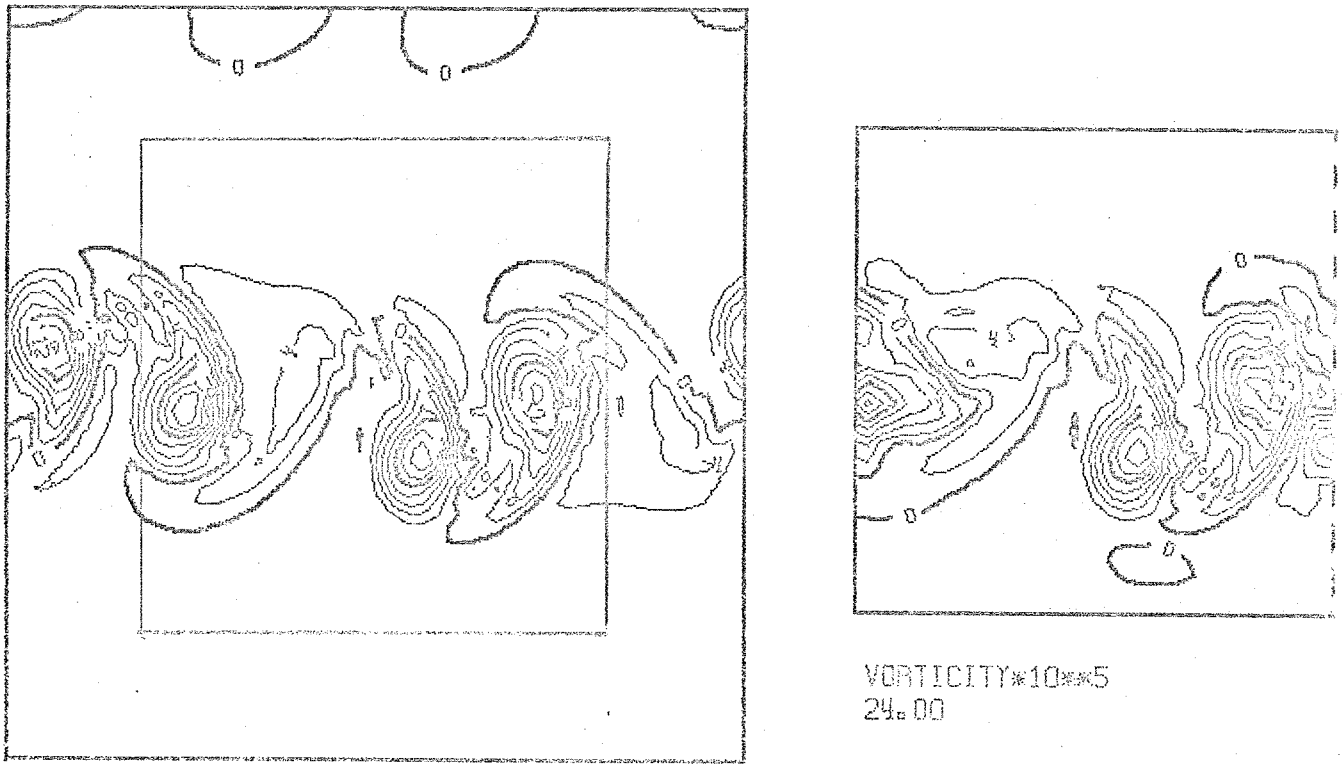

Figure 11.

Fine mesh cyclic vorticity (sec^{-1}) at +24 hour (left). Limited area vorticity at +24 hour (right), same integration as in fig.9.

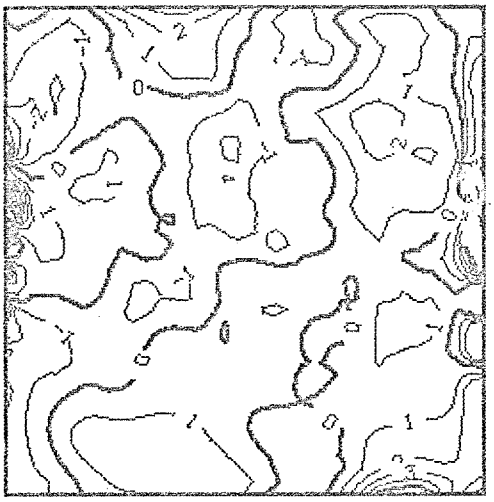

DIVERGENCE*10**6
48.00

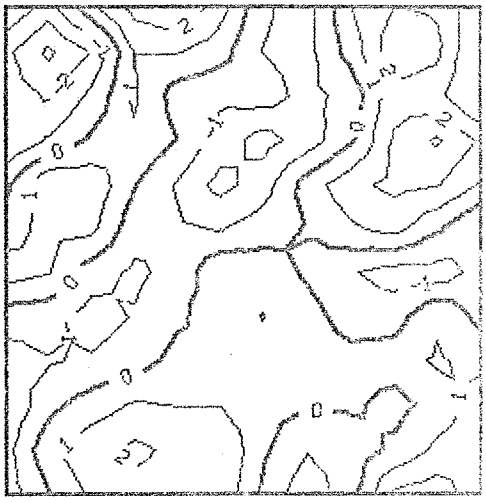

DIVERGENCE*10**6
48.00

Figure 12.

+48 hour divergence (sec^{-1}), same run as fig.10.
Left: limited area. Right: coarse mesh forcing.

yield continuous derivatives at the given coarse mesh points. In the present 1:3 ratio between the meshlengths, these discontinuities cause $3\Delta s$ noise, particularly in the divergence, which of course is obtained as a difference. In figure 13a the divergence of the initially generated fine mesh windfield is shown. Selecting every ninth point to form a coarse mesh data set and reinterpolating this set to the fine mesh, produced the divergence seen in figure 13b. The wind components themselves, on the other hand, did not show any short wave interpolation noise after the process, (figure 4). To avoid spurious divergence generation at the interpolation, some scheme yielding continuous derivatives should be used. On such scheme is Fourier-interpolation, and another is the use of smoothed cubic splines. The latter method produces the divergence in figure 13c.

4. Conclusion

From these experiments some conclusions on the performance of the simplified version of the relaxation scheme can be made.

The boundaries fully absorb rapidly moving gravity waves generated within the limited area, even with a rather steep relaxation coefficient. Slow meteorological waves with large cross-boundary advections require some more care. The boundary zone should be at least 5 or 6 meshlengths wide and the relaxation coefficient must approach the interior zero value very slowly. Preferably the e-damping time of the relaxation coefficient should be of the same order as the wave frequency at at least a few meshpoints. For mixed Rossby and gravity waves the tanh-shaped profile seems to be a good compromise. Great care has to be taken in the spatial interpolation. Interpolation schemes yielding discontinuous derivatives causes considerable noise in the divergence of the external forcing. Although the divergence does not seem to spread into the interior, it is still unwanted.

In conclusion this very simple boundary treatment is satisfactory for a limited area barotropic model in the sense that it absorbs gravity waves and does not produce computational noise in the overspecified tangential velocities at outflow boundaries.

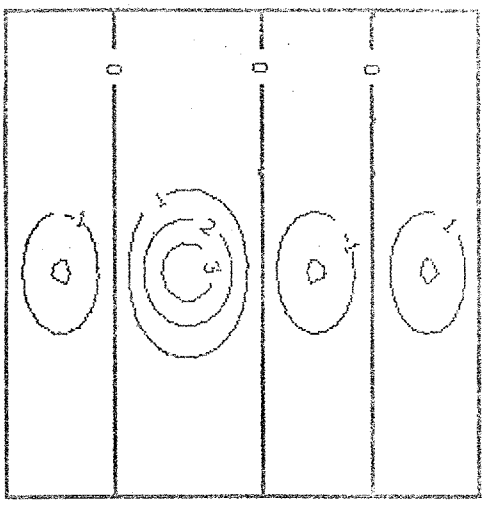

DIVERGENCE*10**6
0.00

Figure 13a.

Divergence (sec^{-1}) of original fine mesh wind field.

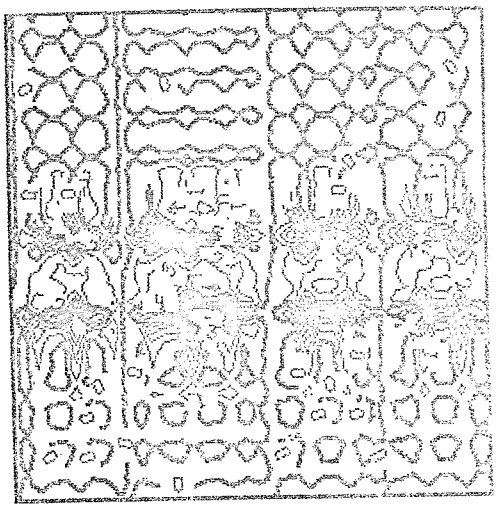

DIVERGENCE*10**6
0.00

Figure 13b.

Divergence of Shapiro-interpolated initial coarse mesh windfield.

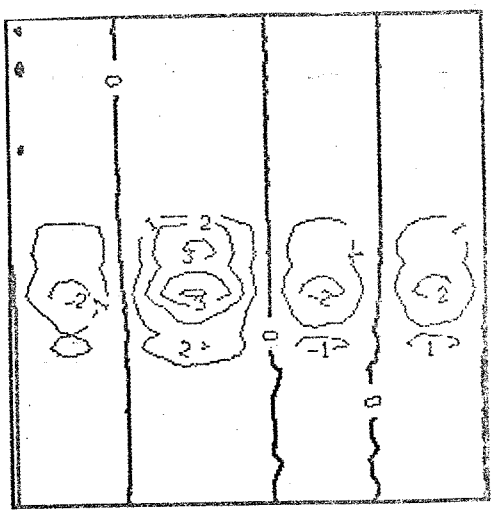

DIVERGENCE*10**6
0.00

Figure 13c.

Divergence of spline-interpolated initial coarse mesh windfield.

References:

Burridge, D., (1977) ECMWF model dynamical formulation Technical Report No.4, ECMWF, Bracknell (in press)

Davies, H.C., (1976) A lateral boundary formulation for multi-level prediction models. Quart. J.R. Met. Soc. (1976), 102, pp. 405-418.

Kreiss, H-O. & J. Oliger, (1973) Methods for the approximate solution of time dependent problems. GARP Publication Series, No.10, WMO-ICSU.

Miyakoda, K. & A. Rosati, (1977) One-way nested grid models: the interface conditions and the numerical accuracy. GFDL/NOAA (to be published)

Shapiro, R., (1973) A high order interpolation procedure for use in fine-mesh limited area models. AFCRL-TR-73-0543. Air Force Cambridge Research Laboratories, Bedford, Mass.

Sundström, A., (1973) Theoretical and practical problems in formulating boundary conditions for a limited area model. Report DM-9, Institute of Meteorology, University of Stockholm.

Figures:

1 : Geopotential (m^2sec^2) at 10 minutes intervals. Without boundary relaxation. 40 x 40 points, meshsize 10 km, timestep 10 sec.

2 : As figure 1 but with boundary relaxation. The isoline marked 90.0 denotes 1% of the initial amplitude.

3 : Disturbance kinetic energy as function of time. Without relaxation (full line) and with relaxation (dashed line).

4 : Initial fields in the full cyclic area. The limited area is outlined by the inner frame. Winds in $msec^{-1}$. Geopotential in m^2sec^2.

5 : +48 hour forecast in the full cyclic area. Fine mesh 100 km, timestep 100 sec. The limited area is outlined by the inner frame. Winds in $msec^{-1}$. Geopotential in m^2sec^2.

6 : +48 hour forecast, limited area. Without boundary relaxation. Other data as fig.5.

7 : +24 hour and +48 hour vorticity in sec^{-1}. Without relaxation.

8a : Tangential velocity ($msec^{-1}$) at the outflow boundary of one row of gridpoints. Dashed line interpolated forcing. Full line limited area forecast without relaxation.

8b : As fig. 8a but with relaxation. Relaxation coefficient linear.

8c : As fig. 8b but tanh-shaped relaxation coefficien..

9 : +24 hour limited area forecast (upper part) with tanh-relaxation.
+24 hour coarse mesh forecast over the limited area (lower part). Isolines as in fig.5.

10 : As fig. 9 but +48 hour.

Figures: (cont..)

11 : Fine mesh cyclic vorticity (sec^{-1}) at +24 hour (left). Limited area vorticity at +24 hour (right), same integration as in fig.9.

12 : +48 hour divergence (sec^{-1}), same run as fig.10. Left: limited area. Right: coarse mesh forcing.

13a : Divergence (sec^{-1}) of original fine mesh wind field.

13b : Divergence of Shapiro-interpolated initial coarse mesh windfield.

13c : Divergence of spline-interpolated initial coarse mesh windfield.

EUROPEAN CENTRE FOR
MEDIUM RANGE WEATHER
FORECASTS

Research Department (RD)

Internal Report No.3

No.1 Users Guide for the G.F.D.L. Model
(November 1976)

No.2 The Effect of Replacing Southern Hemispheric Analyses by Climatology on Medium Range Weather Forecasts
(January 1977)

No.3 Test of a Lateral Boundary Relaxation Scheme in a Barotropic Model
(February 1977)